Council on Tall Buildings and Urban Habitat
CTBUH Research Paper
ctbuh.org/papers

Title: **Flexural Capacity of the Encased(Slim Floor) Composite Beam with Deep Deck Plate**

Authors:
Tae-Sup Moon, Researcher, Korea Institute of Construction Technology
Myong-Keun Kwak, Senior Researcher, Korea Institute of Construction Technology
Byung-Wook Heo, Chief Researcher, Korea Institute of Construction Technology
Kyu-Woong Bae, Vice President, Korea Institute of Construction Technology
Keung-Hwan Kim, Professor, Hanyang University

Subject: Structural Engineering

Keywords: Concrete
Shear
Structure

Publication Date: 2004

Original Publication: CTBUH 2004 Seoul Conference

Paper Type:
1. Book chapter/Part chapter
2. Journal paper
3. **Conference proceeding**
4. Unpublished conference paper
5. Magazine article
6. Unpublished

© Council on Tall Buildings and Urban Habitat / Tae-Sup Moon; Myong-Keun Kwak; Byung-Wook Heo; Kyu-Woong Bae; Keung-Hwan Kim

# Flexural Capacity of the Encased(Slim Floor) Composite Beam with Deep Deck Plate

Myong-Keun Kwak[1], Byung-Wook Heo[2], Kyu-Woong Bae[3], Keung-Hwan Kim[4], Tae-Sup Moon[5]

[1] Researcher, Korea Institute of Construction Technology(KICT)
[2] Senior Researcher, Korea Institute of Construction Technology(KICT)
[3] Chief Researcher, Korea Institute of Construction Technology(KICT)
[4] Vice President, Korea Institute of Construction Technology(KICT)
[5] Professor, Department of Architectural Engineering, Hanyang University

**Abstract**

The advantages of composite construction are now well understood in terms of structural economy, good performance in service, and ease of construction. However, these conventional composite construction systems have some problems to apply steel framed buildings due to their large depth. So, in this study we executed an experimental test with "Slim Floor" system which could reduce the overall depth of composite beam. Slim Floor system is a method of steel frame multi-story building construction in which the structural depth of each floor is minimized by incorporating the steel floor beams within the depth of the concrete floor slab. Presented herein is an experimental study that focuses on flexural behavior of the partially connected slim floor system with asymmetric steel beams encased in composite concrete slabs. Eight full-scale specimens were constructed and tested in this study with different steel beam height, slab width, with or without shear connection and concrete topping thickness. Observations from experiments indicated that the degree of shear connection without additional shear connection was 0.53~0.95 times that of the full shear connection due to an inherent mechanical and chemical bond stress.

**Keywords**: Slim Floor, Composite Beam, Deep Deck Plate, Shear Connector, Partially Connected Composite Beam

## 1. Introduction

Steel framed buildings usually adopt the composite construction system, a method that optimizes the effectiveness taking advantage of good properties of any materials, and that tends to be increasingly applied to constructions such as columns, beams, floor systems. For example, the composite beam system, in which a beam incorporates with a composite deck plate, is applied to most floor systems of steel framed buildings.

Two popular composite beams are the encased composite beam and the exposed composite beam. In the encased composite beam, a steel beam is fully encased in concrete, as shown in Fig 1(a). In the exposed composite beam, a composite slab is situated on the top of a steel beam, leading to maximizing moment capacity, as shown in Fig 1(b). If satisfying the requirements of concrete cover, the encased composite beam provides fully composite behavior over the structure without shear connectors, and has a good property against earthquakes but bad constructive performance and high costs, leading to rare applications in Korea.

The exposed composite beam has good properties of flexural capacity and constructive effectiveness, so it is applied to floor systems of steel framed building at many construction sites. However, it also has higher floor heights of buildings due to slabs located on the top of steel beams, and several problems over fire protection and local buckling at the upper compressive flange and web of steel beams. The height of buildings is a decisive factor for selecting the structural system of buildings especially in city areas, and therefore a lot of efforts have been poured into studies on reducing the height of buildings at home and abroad.

Recently in Europe, as shown in Fig 2, the slim floor method is being widely developed and used, a method that uses asymmetric steel beams with a deeper deck plate or a precast hollow slab as the floor slab. (Mullett,1998)

However, for the partially connected composite beam with a plate welded to the lower flange of a steel beam, references are not available enough for the horizontal shear force of steel beams and the adhesion of concrete itself, and related standards are not prepared for the partially connected composite beam.

This study focuses on partially composite beam using asymmetric steel beams welded with a wider plate to the lower flange, and a composite slab with a

Contact Author: Myong-Keun Kwak, Researcher, Korea Institute of Construction Technology, 2311 Daehwa-dong Ilsna-ku Koyang-shi Koungki-do, Rep. of Korea
Tel: +82-31-9100-358 Fax: +82-31-9100-361
e-mail: mkkwak@kict.re.kr

newly developed deep deck plate. A variety of experimental specimens were made and tested in order to evaluate properties of flexural and adhesive behavior.

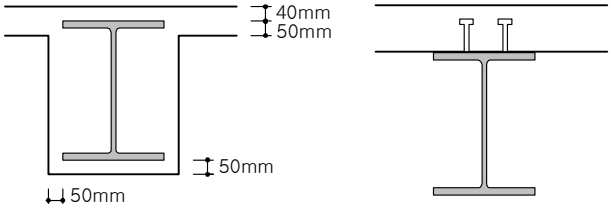


(a) Encased Type (b) Exposed Type

**Fig. 1.** Conventional Composite Beam

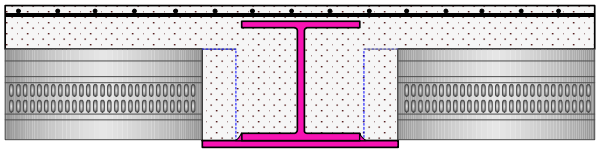

**Fig. 2.** Slim Floor Composite Beam

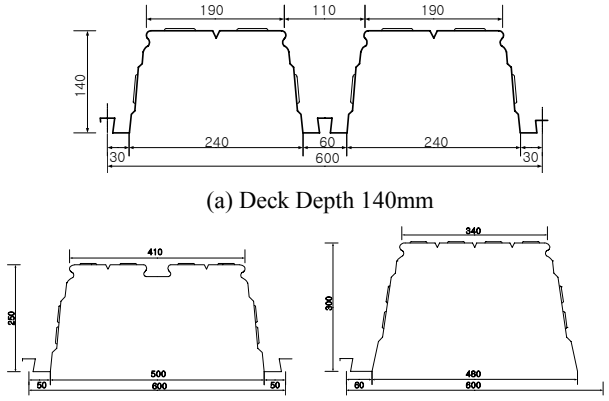


(a) Deck Depth 140mm

(a) Deck Depth 250mm (b) Deck Depth 300mm

**Fig. 3.** Deep Deck Plate

## 2. Flexural Capacity of Encased Composite Beam

### 2.1 Fully Connected Composite Beam

For a fully connected composite beam, the whole section provides flexural capacity if the horizontal shear capacity of shear connectors is greater than the smaller values between the shear capacity of the steel beam and the concrete. The ultimate flexural capacity of the fully connected composite beam when may be calculated with applying plastic analysis by the equivalent stress block of concrete, according to LRFD, U.S.A (AISC, 1999), as shown in Fig 4. Assumptions of the plastic analysis are as follows:

① Concrete does not resist tensile stress but compressive stress only.

② The distribution of compressive stress within concrete structures at the ultimate capacity is the rectangular stress block, $0.85 f_{ck}$.

③ The distribution of compressive and tensile stress of steel beams at the ultimate capacity is the rectangular stress block, $f_y$.

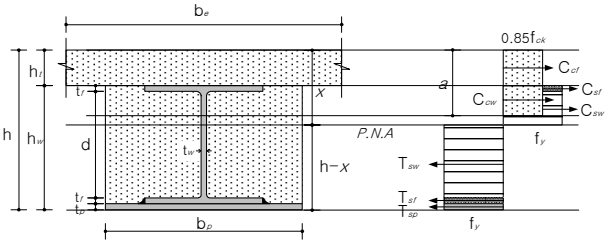


**Fig. 4.** Stress Distribution of encased fully composite beam

If the neutral axis of a composite section forced by positive moment is located at the web surface of steel beams, the compressive force, $C$ may be obtained by summing up compressive forces onto the concrete slab and web, $C_c (= C_{cf} + C_{cw})$, and compressive forces onto the flanges and web of a steel beam, $C_s (= C_{sf} + C_{sw})$, see Equation (1).

$$C = C_{cf} + C_{cw} + C_{sf} + C_{sw} \tag{1}$$

The tensile force, $T$ may be obtained by summing up tensile force onto the web of a steel beam, $T_{sw}$, tensile force onto the flange, $T_{sf}$, and tensile force onto the plate, $T_{sp}$, see Equation (2).

$$T = T_{sw} + T_{sf} + T_{sp} \tag{2}$$

With equilibrium of $C = T$, the length from the top to the neutral axis, $x$ may be provided by Equation (3).

$$x = \frac{A_p f_y + (h + h_t - t_p) t_w f_y - 0.85 f_{ck} \left[ (b_e - b_p) h_t + (h_t + t_f) t_w - A_f \right]}{0.85 f_{ck} \beta_1 (b_p - t_w) + 2 t_w f_y} \tag{3}$$

Therefore, the ultimate flexural moment capacity on fully connected composite section may be provided by Equation (4).

$$M = T_{sp}(h - x - \frac{t_p}{2}) + T_{sf}(h - x - t_p - \frac{t_f}{2}) + T_{sw}\frac{(h - x - t_p - t_f)}{2} + C_{sw}\frac{(x - h_t - t_f)}{2} + C_{sf}(x - h_t - \frac{t_f}{2}) + C_{cw}[x - (\frac{h_t + a}{2})] + C_{cf}(x - \frac{h_t}{2}) \tag{4}$$

where,

$A_s$ : area of flange
$A_p$ : area of flange plate
$b_e$ : effective width of concrete slab
$a$ : effective thickness of concrete slab
$b_p$ : width of flange plate
$t_p$ : thickness of flange plate
$f_{ck}$ : compressive strength of concrete
$f_y$ : yield stress of steel

$h$ : height of composite beam
$h_t$ : thickness of concrete slab
$t_f$ : flange thickness
$t_w$ : web thickness
$x$ : distance from top of concrete to neutral axis of composite beam
$\beta_1$ : 0.85

### 2.2 Partially Connected Composite Beam

If the horizontal shear capacity of a composite beam, $F_{sb}$ is less than the horizontal shear force loaded onto components, $R_c$ , that is $F_{sb} \langle R_c$ , the flexural capacity of composite section is decreased because two members which may slip each other at the interface. At this point, the plastic resisting moment adopts reduced compressive force on the concrete slab, $F_{sb}$ . Likewise, in current designs of the partially connected composite beam, the flexural capacity is calculated using reduced compressive force, the same method as the fully connected composite beam.

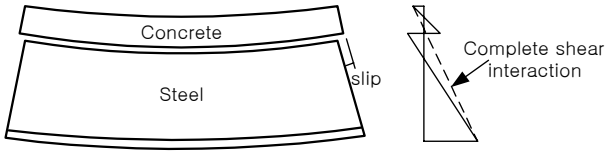


(a) Deformed Shape (b) Strain Distribution

**Fig. 5.** Behavior of Partially Composite Beam

Current design methods of the partially connected composite beam have taken the composite action with shear connectors only. If not considering shear connectors, the designs have adopted the encased composite beam, SRC beam, or the bare steel beam only. LRFD of U.S.A (AISC, 1993) used Equation (5) to calculate the effective stiffness of composite beams.

$$EI_p = EI + \sqrt{\frac{N}{N_f}}(EI_f - EI_s) \tag{5}$$

$N/N_f$ : Shear Interaction factor
$EI_s$ : flexural stiffness of steel beam
$EI_f$ flexural stiffness of fully composite beam
$EI_p$ : flexural stiffness of partially composite beam

BS5950 Part 1 of Britain (D.L. Mullett, 1998) applied the linear relationship of Equation (6) to determine design resisting moment on partially connected composite beams, $M_d$

$$M_d = M_s + \frac{F_{sb}}{R_c}(M_c - M_s) \tag{6}$$

$M_s$ : plastic moment resistance of steel section
$R_c$ : compressive resistance of concrete section
$F_{sb}$ : longitudinal shear bond force
$M_c$ : plastic moment resistance of composite section
$F_{sb}/R_c$ : Degree of shear connection

In Equation (6), $M_d$ can be replaced by the resisting moment from the experimental result and then the horizontal shear capacity of partially connected composite beams, $F_{sb}$ can be indirectly evaluated by the experimental results, as shown in Equation (7).

$$F_{sb} = R_c \frac{(M_d - M_s)}{(M_c - M_s)} \tag{7}$$

$$F_{sb} = [s(B_f + t_f + d) - t_w] f_w L/4 \tag{8}$$

It is assumed that the horizontal shear capacity results from the shear bond stress, $F_{sb}$ , which uniformly acts around both the web surface and the upper flange of asymmetric steel beam section. For beams under loading at 2 concentrated points, Equation (8) presents the maximum compressive force, $F_{sb}$ onto the slab at the center of beam considering elastic shear flow.

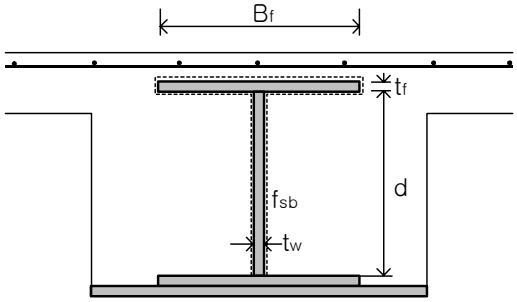


**Fig. 6.** Shear Bond Surface of Steel Beam

Shear bond stress, $f_{sb}$ may be obtained by Equation (9), incorporated by Equation (7) and (8).

$$f_{sb} = \frac{R_c \frac{(M_d - M_s)}{(M_c - M_s)}}{[2(B_f + t_f + d) - t_w] L/4} \tag{9}$$

## 3. Experiment

### 3.1 Experimental Plan

Full-scale specimens for simple steel beams spanned 6m were tested, in order to evaluate the flexural behavior of slim floor composite beams of which the surfaces of web are encased in concrete. Total 8 specimens were constructed taking account of following factors; mainly the depths of steel beams, 200mm, 250mm, 300mm, and the depths of decks for composite slabs, 140mm, 250mm, 300mm, as well as loading types (concentricity and eccentricity), with or without studs, and the effective width of slab (span/8 and span/4). See Table 1 and Fig 7. Wired meshes of Ψ 6-100×100 reinforced the compressive concrete at the upper slab. Then shear studs of Ψ 19-70 were placed in 2 rows, spacing @300.

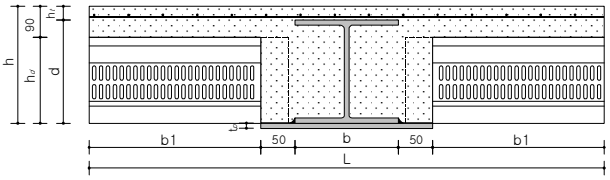


(a) SB200, SB300-A, B, C
(Loading Type, Effective Width of Slab)

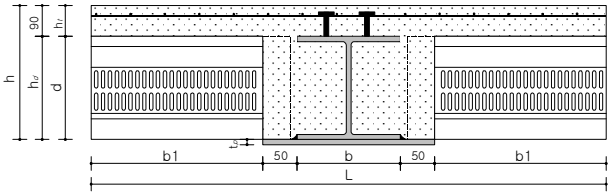


(b) SB-250A, B, SB300-D, E
(With or Without Shear Connector)

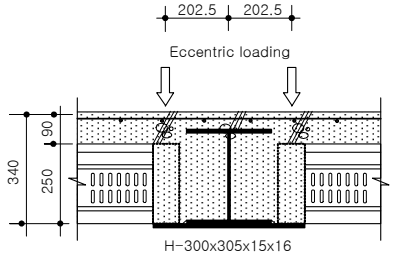


(c) SB300-C (Eccentric loading)

**Fig. 7.** Shape and Dimension of Specimens

### 3.2 Loading and Measurement Methods

Loads took account into displacement control and loading speed was 0.05 mm/sec. 3400kN capacity hydrostatic actuator were taken as loading machines, as shown in Fig 8 and 10. The loads were applied at 2 points L/4 shear span apart from the supports, maximizing the effectiveness of equivalent distributed loads.

In order to measure the displacement at the loading points and the center of span, 3 displacement transdusers (LVDT 200mm : D1, D2, D3) were installed at the lower part of specimens. In order to measure the amount of end-slip generated at the boundary between a steel beam and a concrete slab, 2 displacement transdusers (LVDT 100mm : D4, D5) were installed at both ends, as shown in Fig 9. In order to measure strain by loads, W.S.G (Wire Strain Gauge) were attached at the center of spans of specimens, as shown in Fig 11.

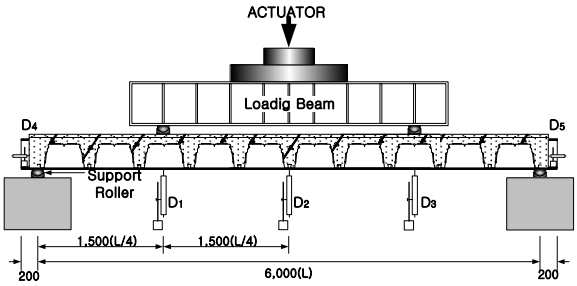


**Fig. 8.** Load and Measurement Methods

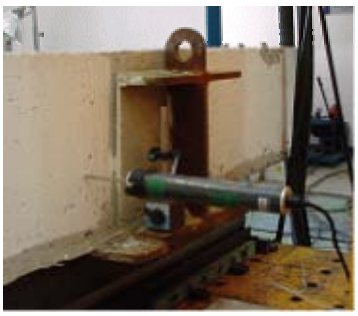

**Fig. 9.** Measurement of End Slip

**Fig. 10.** Test Set-up

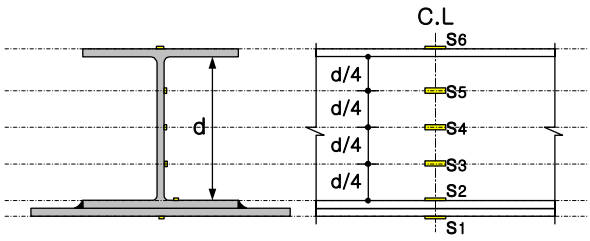


**Fig. 11.** Positions of W.S.G

**Table 1.** Details of Specimens

| specimen | h | $h_d$ | $h_t$ | d | H-section | $t_p$ | b | $b_1$ | L | Shear Stud | Loading type | Note |
|---|---|---|---|---|---|---|---|---|---|---|---|---|
| SB200 | 230 | 140 | 30 | 200 | H-200×200×12×8 | 15 | 200 | 550 | 1500 | without | concentric | Asymmetric Steel Beam + Deep Deck |
| SB250-A | 340 | 250 | 90 | 250 | H-250×250×14×9 | | 250 | 525 | 1500 | with | concentric | |
| SB250-B | | | | | | | | | | without | | |
| SB300-A | | | 40 | 300 | H-300×305×15×15 | | 305 | 525 | 1500 | without | concentric | |
| SB300-B | | | | | | | | 122.5 | 750 | | | |
| SB300-C | | | | | | | | 525 | 1500 | | eccentric | |
| SB300-D | 390 | 300 | 90 | 300 | H-300×305×15×15 | | 305 | 497.5 | 1500 | with | concentric | |
| SB300-E | | | | | | | | | | without | | |

### 3.3 Material Property

Test specimens for tension on steels were made according to KS B 0801 (Standards for tensile test specimens of metal materials), in order to analyze mechanical properties of the steel used for experimental specimens. For deck plates, normal hot dip zinc coating steel plates were used and H-section and plates, SS400 steels were used. Test results in Table 2 includes yield strength, tensile strength and yield ratio.

**Table 2.** Test Resuts of materials

| Speci-men | thickness (mm) | $\sigma_y$ (Mpa) | $\sigma_u$ (Mpa) | $\sigma_y/\sigma_u$ | $\varepsilon_y$ ($\times 10^{-6}$) | $\varepsilon_{st}$ ($\times 10^{-6}$) | $E_{st}$ (Mpa) | $El_o$ (%) |
|---|---|---|---|---|---|---|---|---|
| Deck | 1.2 | 245.0 | 338.1 | 0.72 | 2157 | 16969 | 1147 | 35 |
| | 1.4 | 301.8 | 365.5 | 0.82 | 1756 | 35580 | 1460 | 33 |
| Flange | 12 | 251.9 | 396.9 | 0.63 | 2140 | 22177 | 3205 | 37 |
| | 14 | 276.4 | 426.3 | 0.65 | 2800 | 24650 | 3616 | 41 |
| | 15 | 260.7 | 400.8 | 0.65 | 1562 | 11479 | 3009 | 38 |
| Web | 8 | 259.7 | 399.8 | 0.65 | 1850 | 26983 | 4567 | 37 |
| | 9 | 343.0 | 459.6 | 0.77 | 2500 | 22654 | 3842 | 40 |
| | 15 | 240.1 | 362.6 | 0.66 | 2700 | 10255 | 2685 | 37 |
| Plate | 15 | 260.7 | 398.9 | 0.65 | 1762 | 16730 | 2881 | 38 |

The design strength of concrete was 23.5MPa, and total 12 specimens were made by grouping compressive strength test pieces into 4 triads based on the number of remicon inputs, according to KSF 2404. Average mechanical properties of 12 specimens from the concrete compressive strength tests are presented in Table 3.

**Table 3.** Test Results of Concrete

| $f_{ck}$ (MPa) | $E_c$ (MPa) | Slump (cm) |
|---|---|---|
| 24.01 | $1.77 \times 10^4$ | 12 |

### 3.4 Test Results of Composite Beams

Table 4 shows test results for flexural capacities of encased composite beams. In Table 4, the values of initial cracks and slip loads represent changing points of initial tangential stiffness after crack and points of initial slip in the load-end slip curves as shown in Fig 12, respectively. In addition, initial stiffness, stiffness after crack and stiffness after slip are represented.

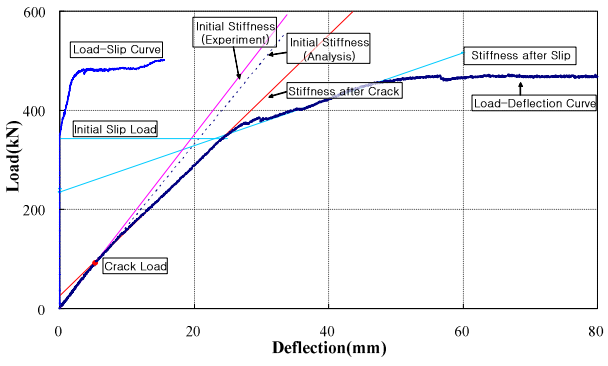


**Fig. 12.** Definition of strength and stiffness

Fig 13 shows failure states of specimens for encased composite beams, by specimens. As a test result, the specimens without shear connectors presented ductile behavior regardless of depth of the steel beam. All specimens are followed pre-crack, post-crack and slip steps in order, and after the yield, loads gradually got increased to the maximum load level, and from this point the loads gradually decreased without sudden drop of the load.

The initial crack appeared along with the outer edge of the upper flange of steel beams on the top surface of the slab, in the length direction of the loading point towards the support.

After the initial crack, flexural cracks appeared near the area of loading point at the side of the compressive concrete.

With loads increased, the slip of steel beams and concrete appeared before and after yielding on lower tensile flange of the steel beam. Then, tensile cracks in the length direction on the surface of upper concrete, and diagonal cracks around the loading points got expanded, and reached the maximum load. Finally, the test was ended by crushing of the upper concrete on the loading point.

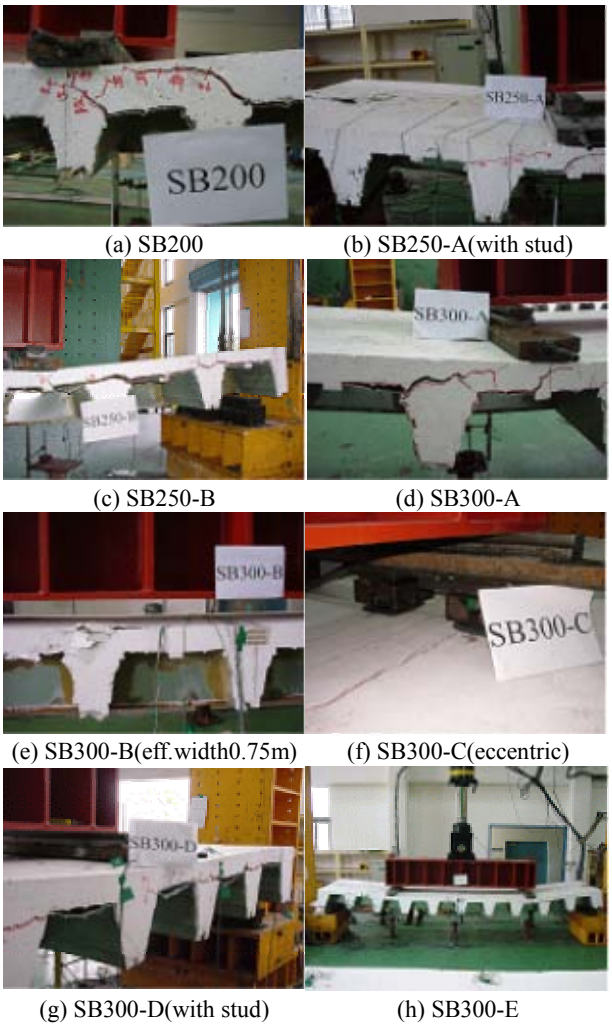


(a) SB200 (b) SB250-A(with stud)

(c) SB250-B (d) SB300-A

(e) SB300-B(eff.width0.75m) (f) SB300-C(eccentric)

(g) SB300-D(with stud) (h) SB300-E

**Fig. 13.** Test result view after failure

**Table 4.** Test Results

| specimen | initial crack load $P_c$(kN) | initial crack load $P_s$(kN) | yield load $P_y$(kN) | | | ultimate load $P_u$(kN) | | | Stiffness(kN/㎜) initial stiffness ($K_i$) | | | stiffness after crack ($K_c$) | | | stiffness after slip | | deflection Δ (㎜) | | |
|---|---|---|---|---|---|---|---|---|---|---|---|---|---|---|---|---|---|---|---|
| | | | $P_{ye}$ | $P_{yt}$ | $P_{ye}/P_{yt}$ | $P_{ue}$ | $P_{ut}$ | $P_{ue}/P_{ut}$ | $K_{ie}$ | $K_{it}$ | $K_{ie}/K_{it}$ | $K_{ce}$ | $K_{ct}$ | $K_{ce}/K_{ct}$ | $K_s$ | $K_s/K_{ce}$ | $\Delta_y$ | $\Delta_u$ | $\Delta_u/\Delta_y$ |
| SB200 | 128.4 | 363.6 | 354.8 | 343.0 | 1.03 | 506.7 | 548.8 | 0.92 | 17.3 | 15.6 | 1.10 | 12.64 | 12.74 | 1.00 | 4.6 | 0.36 | 25.7 | 191.6 | 7.45 |
| SB250-A | 207.8 | - | 876.1 | 989.8 | 0.86 | 1018.2 | 1092.7 | 0.92 | 49.5 | 44.6 | 1.11 | 34.40 | 39.10 | 0.88 | 26.7 | 0.78 | 29.3 | 59.2 | 2.02 |
| SB250-B | 206.8 | 413.6 | 669.3 | 989.8 | 0.68 | 920.2 | 1092.7 | 0.83 | 41.8 | 44.6 | 0.94 | 28.22 | 39.10 | 0.72 | 11.6 | 0.41 | 30.2 | 172.5 | 5.71 |
| SB300-A | 211.7 | 698.7 | 1020.2 | 1146.6 | 0.89 | 1343.6 | 1395.5 | 0.96 | 51.7 | 51.9 | 1.00 | 44.88 | 44.88 | 1.0 | 19.4 | 0.43 | 29.0 | 171.0 | 5.90 |
| SB300-B | 218.5 | 725.2 | 1078.0 | 1048.6 | 1.03 | 1293.6 | 1230.9 | 1.05 | 37.0 | 41.3 | 0.90 | 31.65 | 33.61 | 0.94 | 22.4 | 0.71 | 38.0 | 178.0 | 4.68 |
| SB300-C | 272.4 | 729.1 | 1085.8 | 1146.6 | 0.95 | 1280.9 | 1395.5 | 0.91 | 41.0 | 51.9 | 0.79 | 40.96 | 44.88 | 0.91 | 22.1 | 0.54 | 33.2 | 183.6 | 5.53 |
| SB300-D | 399.8 | - | 1551.3 | 1313.2 | 1.18 | 1654.2 | 1542.5 | 1.07 | 59.4 | 70.2 | 0.85 | 42.04 | 59.88 | 0.70 | 39.3 | 0.93 | 38.6 | 48.2 | 1.25 |
| SB300-E | 262.6 | 571.3 | 1156.4 | 1313.2 | 0.88 | 1523.9 | 1542.5 | 0.98 | 61.4 | 70.2 | 0.87 | 42.24 | 59.88 | 0.71 | 22.4 | 0.53 | 36.7 | 136.0 | 3.71 |

e : experimental value, t : theoretical value

For specimens with studs, the load went through pre-crack, post-crack and yield steps, and soon reached the maximum load level. Then, the test was ended in early stage by crushing of the upper compressive concrete.

Fig 14 shows the load-displacement relationship by specimens for encased composite beams. Furthermore, it shows analysis values of flexural capacity of bare steel and composite beams and end-slip curve at both ends.

For SB200 with the depth of 200mm of steel beams, the initial stiffness continued to 88kN, and behaved linearly after lower tensile concrete crack to slip load, 333kN, and then the stiffness suddenly decreased due to the slip and yield of tensile steel beams. Then at the slip load, 451kN, the displacement was increased without increasing of the load and finally the test was ended at the maximum load.

For SB250-B, the initial stiffness continued to 196kN, and, after the slip appeared, the displacement was increased without increasing of the load around the limit load of slip resistance, 784kN.

SB250-A and SB300-D which have shear studs on the upper flange of steel beams, because the end-slip at the ends was restrained, the strength rapidly increased after the yield point without decrease of the stiffness. The maximum load was reached when the deflection was reached around L/120(50mm) of the span, and the test was ended earlier due to the crushing of the upper concrete slab. Deflection at the end point of the test was about L/60(100mm). The initial crack was produced along with the surface of concrete on the studs, along length direction of beams. The slip hardly occurred until the maximum load.

SB300-A, B and C, all with the depth of steel beams, 300 mm and the depth of decks, 250 mm, hardly showed influence of loading types. The specimen SB300-B, with the effective width 0.75m, reached the yield point after the initial slip without rapid decrease of the stiffness. It showed very stable behaviors similar to the bare steel beams from the yield point to the maximum load.

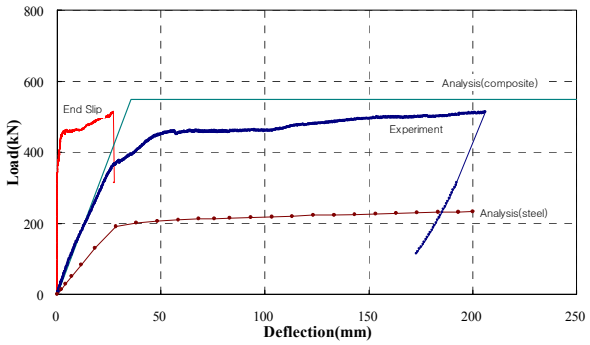


(a) SB200 (Deck Depth 140mm)

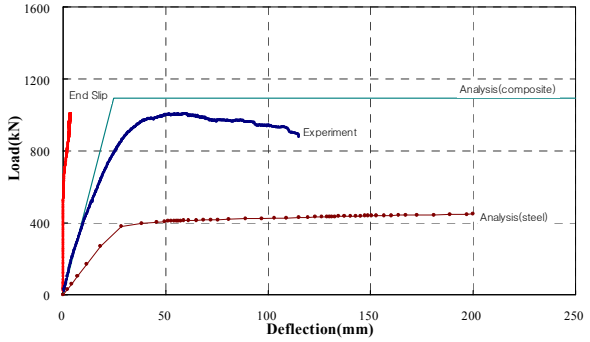


(b) SB250-A (With Stud, Deck Depth 250mm)

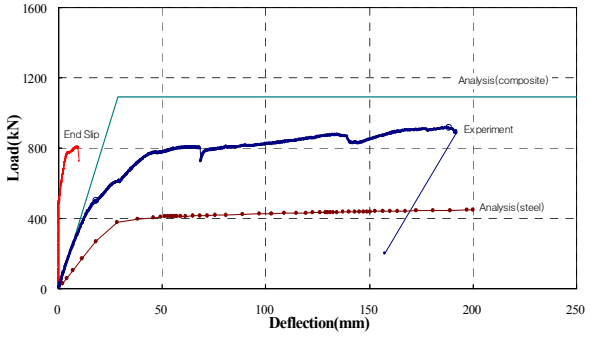


(c) SB250-B (Deck Depth 250mm)

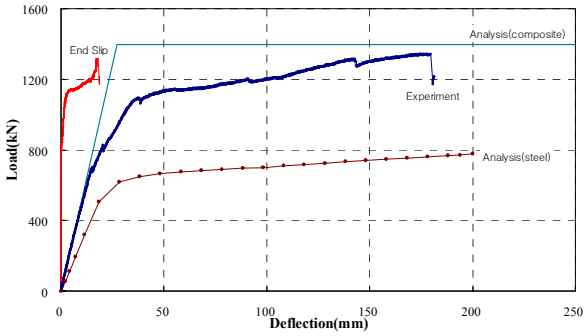


(d) SB300-A (Deck Depth 250mm)

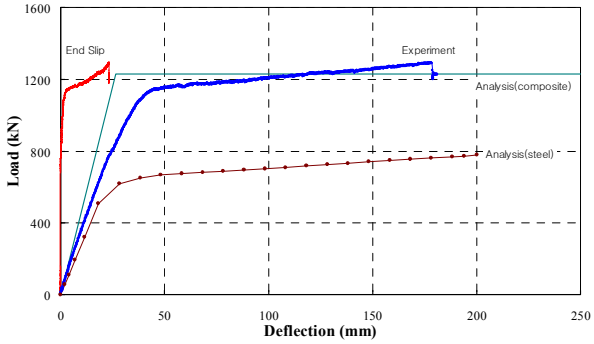


(e) SB300-B(eff. width 0.75, deck depth 250mm)

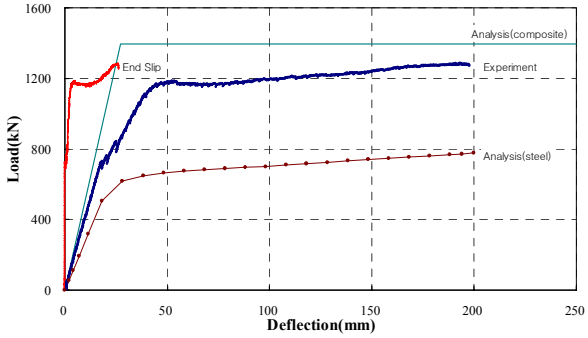


(f) SB300-C(eccentric loading, deck depth 250mm)

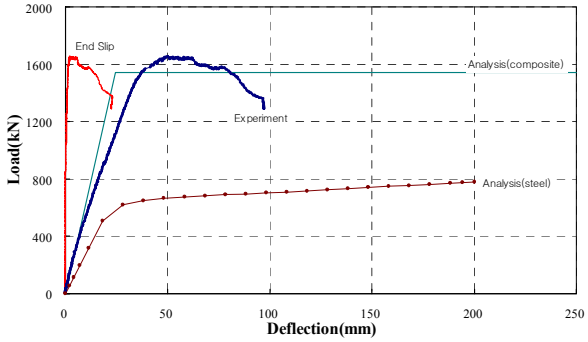


(g) SB300-D(with stud, deck depth 300mm)

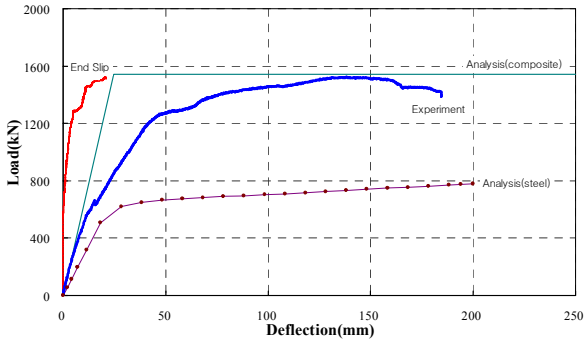


(h) SB300-E(without stud, deck depth 300mm)

**Fig. 14.** Load-Displacement Relationship for specimens

## 4. Analysis of Test Results and Discussion

### 4.1 Comparison of Stiffness and Strength

Fig 15 presented a comparison of the stiffness and ultimate load of encased composite beams with those of bare steel beams. The specimens without studs had 1.11 to 2.52 times greater stiffness than bare steel beams, and the maximum load, 1.65 to 2.18.

Especially for SB300-E with the depth of upper concrete topping, 90mm, the neutral axis neared to the concrete slab, so the slip was produced earlier since the bond strength was reduced by cracked tensile concrete, consequently leading to sudden drop of the strength.

In Figure 16, the yield and ultimate loads from the analytical value were compared with experimental results. For specimens without studs, the ratio of analytical yield loads and test results were 0.91 in average, and the ultimate load of analytical values were 0.84 to 1.05 times greater than the experimental values, since the shear bond effect in the steel beams and the concrete themselves provided great composite action even though no shear studs installed.

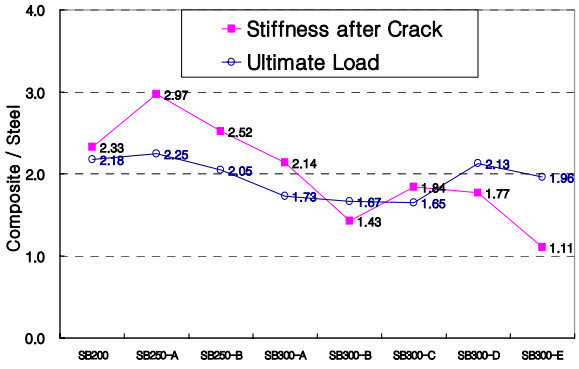


**Fig. 15.** Stiffness & Strength against Steel Beam

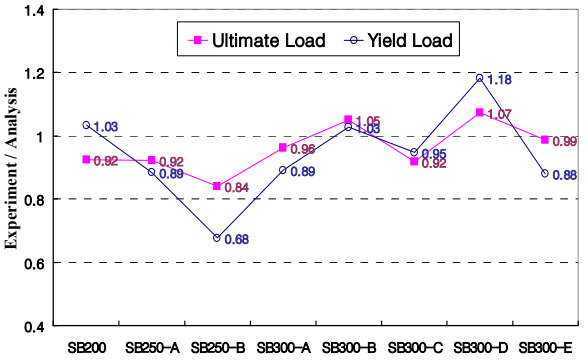


**Fig. 16.** Comparison of test results and analyzed values

### 4.2 Loads-End Slip Behavior

In Fig 17, the load-slip relationship was presented. For SB250-A and SB300-D, both with studs, the slip stiffness was very high with the amount of slip less than 3mm at the maximum load level, but the loads suddenly dropped due to brittle crushing due to restrained slips at the ends.

For specimens without studs, the initial slip load and the stiffness after slip were proportioned linearly for the bond area of steel beams. Especially for a specimen with the depth of 300mm steel beam, the stiffness after the slip is almost constant values regardless of the loading type and the effective width of concrete slab.

For SB300-E specimen with the depth of concrete topping 90mm, the maximum load was greatly increased, but the initial slip load was relatively reduced since the neutral axis of the composite beam was positioned on the upper part of steel beam and then most encased concrete around the web of the steel beam lost its adhesion due to tensile cracks.

The relationship between the initial slip load and the bond length is presented in Fig 18. As a result of comparison, the initial slip load greatly depends on the bond area of steel beams and the depth of concrete cover of upper flanges.

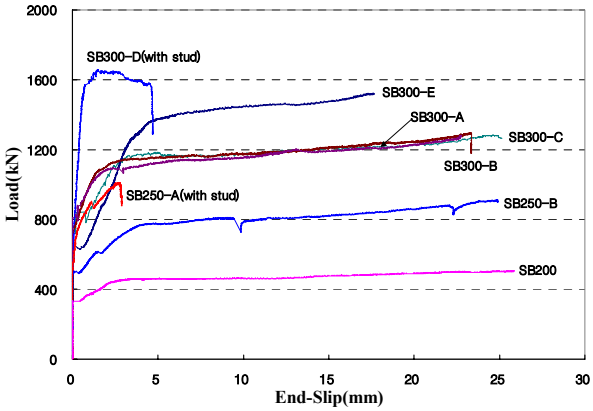


**Fig. 17**. Load-end slip Relationship

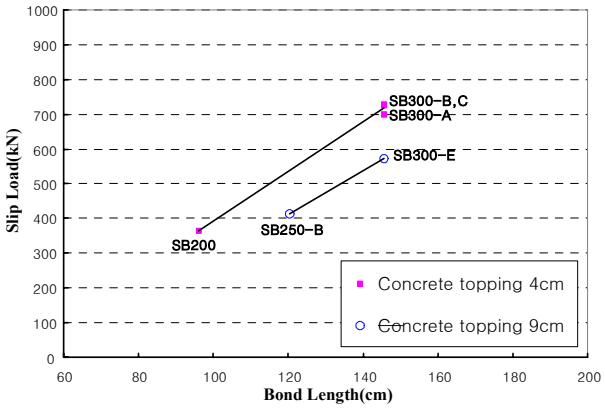


**Fig. 18.** Comparison of Load for Initial end Slip

### 4.3 Distribution of Strain

In Fig 19, the distribution of strain is presented by positions of the steel beam based on the test results for SB200 specimen. On the diagram, the y-axis is the positions of W.S.G, and the x-axis is the distribution of strain by the loads. The neutral axis shift toward the lower flange of the steel beam due to relative slip on the concrete slab and the steel beam at initial slip load, 333kN.

In Fig 20, the positions of the neutral axis are presented based on the existence of studs according to load values obtained by the load-strain distribution in each specimen. For specimens without studs, the neutral axis moved up to the upper flange due to cracks of lower tensile concrete and suddenly went down to the lower flange due to the occurrence of the slip.

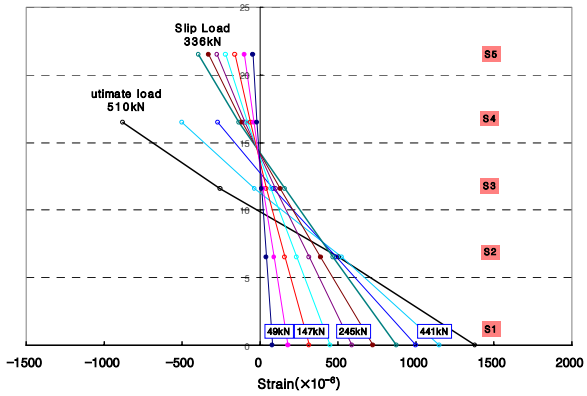


**Fig. 19.** Strain Distribution By Each Load Level

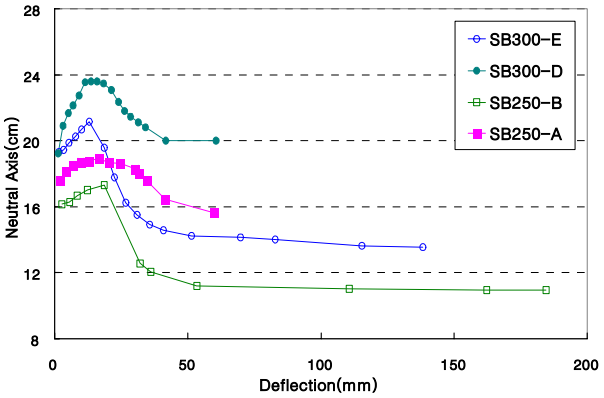


**Fig. 20.** Comparison of Position of Neutral

### 4.4 Evaluation of Composite Ratio

Bond stresses that calculated from the test results with Equation (6) through (9) are listed in Table 5 and Fig 21. The horizontal shear resisting moment, $M_d$, based on the maximum load and the slip load. The composite ratio of composite beams $(F_{sb}/R_c)$ obtained from $F_{sb}$, based on the maximum load of tests. The composite ratios of the encased partially composite beams are presented, as shown in Fig 22. As a result, specimens without additional shear connectors provide relatively good composite ratio, the distribution of 0.53 through 0.95 times.

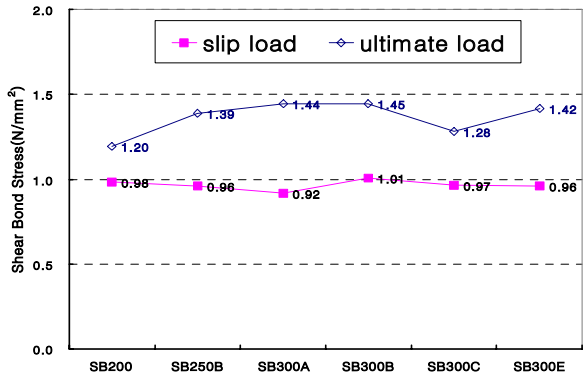


**Fig. 21.** Distribution of Shear Bond Stress for specimens

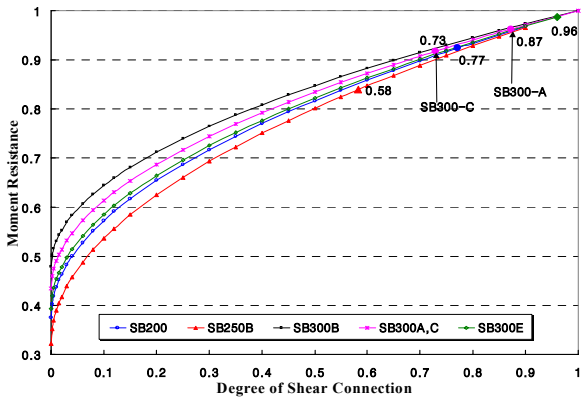


**Fig. 22.** degree of shear connection

**Table 5.** Shear Bond Stress

| Specimen | $R_c$ (kN) | $M_s$ (kN.m) | $M_c$ (kN.m) | $M_d$ (kN.m) | | $F_{sb}$ (kN) | | bond area ($cm^2$) | shear bond stress ($N/mm^2$) | |
|---|---|---|---|---|---|---|---|---|---|---|
| | | | | $M_{dm}$ | $M_{ds}$ | $F_{sbm}$ | $F_{sbs}$ | $A_s$ | $\tau_m$ | $\tau_s$ |
| SB200 | 1587.6 | 174.4 | 411.6 | 380.2 | 343.5 | 1376.9 | 1127.0 | 11520 | 1.20 | 0.98 |
| SB250-B | 2754.8 | 336.2 | 819.3 | 688.0 | 579.2 | 2004.1 | 1381.8 | 14445 | 1.39 | 0.97 |
| SB300-A | 2754.8 | 582.6 | 1046.6 | 1007.4 | 852.6 | 2522.5 | 1597.4 | 17475 | 1.44 | 0.92 |
| SB300-B | 2224.6 | 582.6 | 923.5 | 970.2 | 852.6 | 2529.4 | 1754.2 | 17475 | 1.45 | 1.01 |
| SB300-C | 2753.8 | 582.6 | 1046.6 | 960.4 | 867.3 | 2241.3 | 1685.6 | 17475 | 1.28 | 0.97 |
| SB300-E | 2541.1 | 582.6 | 1157.4 | 1142.7 | 962.9 | 2477.4 | 1675.8 | 17457 | 1.42 | 0.96 |
| average shear bond stress | | | | | | | | | 1.36 | 0.97 |

$\tau$ : $F_{sb}/A_{s,}$ m : maximum load, s : slip load

## 5. Conclusions

The conclusions of the flexural test on the partially connected composite beams are as follows:

(1) For the failure modes of specimens, micro-crack occurred along the length of beam on upper compressive concrete, but the serious concrete separation does not occurred even though the minimum number of horizontal reinforcement.

(2) For partially connected composite beams, the initial slip load appeared linear proportion to the depths of upper concrete topping on steel beams and shear bond area of steel beams.

(3) For encased composite beams, the shear resisting capacity was increased about 50% due to mechanical bond activity by the shape of steel beam even after the beam lost its chemical adhesion.

(4) Shear bond stresses from the test are ranged from 1.20 to 1.45N/mm$^2$ at the maximum loads, and from 0.92 to 1.01N/mm$^2$ at the slip loads. The composite ratios are ranged from 0.53 to 0.96 times in comparison with fully connected composite beams.

## References


Byung-Wook Heo, "Recent Trends in the Development of Slim Floor System", Magazine of the Korean Society of Steel Construction, p124-130, 2003. 6

Jae-Dae Moon, Myong-Keun Kwak, Byung-Wook Heo, Kyu-Woong Bae, Tae-Sup Moon, "An Experimental Study on the Bending Capacity for Slim-Floor Composite Beams", Journal of Korean Society of Steel Construction, p485-492, 2005. 5

The Steel Construction Institute, "Slim Floor Design and Construction", SCI p110, 1992

The Steel Construction Institute, "Slim Floor Construction using Deep Decking", SCI p127, 1993

American Institute of Steel Construction(AISC), "Load and resistance factor specification for structural steel buildings.", 1993

The Steel Construction Institute, "Design of Asymmetric *Slimflor*□ Beams using Deep Composite Decking", SCI P175, 1997

D.L. Mullett, "Composite Floor Systems", The Steel Construction Institute., 1998

Y.C. Wang, "Deflection of steel-concrete Composite Beams with Partial Shear Interaction", Journal of Structural Engineering, 1998